Two-phase flow properties of a sandstone rock for the CO2/water system: Core-flooding experiments, and focus on impacts of mineralogical changes

Jean-Charles Manceau, J. Ma, R. Li, Pascal Audigane, P. X. Jiang, R. N. Xu, Joachim Tremosa, Catherine Lerouge

AGU PUBLICATIONS

Water Resources Research

RESEARCH ARTICLE
10.1002/2014WR015725

Key Points:
- Two-phase flow core flooding is performed on a Chaunoy sandstone sample
- Absolute properties, relative permeability and capillary pressure are assessed
- The impact of mineral dissolution on the measured flow properties is discussed

Supporting Information:
- Supporting Information S1

Correspondence to:
R. Xu,
ruinaxu@mail.tsinghua.edu.cn

Citation:
Manceau, J. C., J. Ma, R. Li, P. Audigane, P. X. Jiang, R. N. Xu, J. Tremosa, and C. Lerouge (2015), Two-phase flow properties of a sandstone rock for the CO_2/water system: Core-flooding experiments, and focus on impacts of mineralogical changes, *Water Resour. Res.*, *51*, 2885–2900, doi:10.1002/2014WR015725.

Received 16 APR 2014
Accepted 28 MAR 2015
Accepted article online 3 APR 2015
Published online 26 APR 2015

Two-phase flow properties of a sandstone rock for the CO_2/water system: Core-flooding experiments, and focus on impacts of mineralogical changes

J. C. Manceau[1,2], J. Ma[1,3], R. Li[1,3], P. Audigane[2], P. X. Jiang[1,3], R. N. Xu[1,3], J. Tremosa[2], and C. Lerouge[2]

[1]Department of Thermal Engineering, Tsinghua University, Beijing, China, [2]BRGM, Orléans, CEDEX 2, France, [3]Key Laboratory for Thermal Science and Power Engineering of Ministry of Education, Beijing, China

Abstract The two-phase flow characterization (CO_2/water) of a Triassic sandstone core from the Paris Basin, France, is reported in this paper. Absolute properties (porosity and water permeability), capillary pressure, relative permeability with hysteresis between drainage and imbibition, and residual trapping capacities have been assessed at 9 MPa pore pressure and 28°C (CO_2 in liquid state) using a single core-flooding apparatus associated with magnetic resonance imaging. Different methodologies have been followed to obtain a data set of flow properties to be upscaled and used in large-scale CO_2 geological storage evolution modeling tools. The measurements are consistent with the properties of well-sorted water-wet porous systems. As the mineralogical investigations showed a nonnegligible proportion of carbonates in the core, the experimental protocol was designed to observe potential impacts on flow properties of mineralogical changes. The magnetic resonance scanning and mineralogical observations indicate mineral dissolution during the experimental campaign, and the core-flooding results show an increase in porosity and water absolute permeability. The changes in two-phase flow properties appear coherent with the pore structure modifications induced by the carbonates dissolution but the changes in relative permeability could also be explained by a potential increase of the water-wet character of the core. Further investigations on the impacts of mineral changes are required with other reactive formation rocks, especially carbonate-rich ones, because the implications can be significant both for the validity of laboratory measurements and for the outcomes of in situ operations modeling.

1. Introduction

Multiphase flow properties of a porous medium give insight into how different fluids can flow in a given porous rock: relative permeability (i.e., effective permeability of one phase) reveals how each phase is displaced in the porous space when other phases are present while capillary pressure refers to the interfacial forces between the fluids and the rock that partly drive the fluids distribution within the pores. The quantification of the multiphase flow through modeling is highly dependent on these two properties and, in this view, the determination of the constitutive relationships of the relative permeability and capillary pressure as a function of the proportion of each fluid is of first importance.

The research effort on CO_2 geological storage during the past decades has given rise to the study of the CO_2/brine system in aquifer rocks, both regarding relative permeability and capillary pressure: *Bennion and Bechu* [2005, 2008, 2010], *Bachu and Bennion* [2008], *Berg et al.* [2013], *Akbarabadi and Piri* [2013], *Chang et al.* [2013], *Wei et al.* [2014], and *Farokhpoor et al.* [2014] performed unsteady state relative permeability measurements while *Perrin and Benson* [2010], *Krevor et al.* [2012], *Zuo et al.* [2012], *Akbarabadi and Piri* [2013], and *Levine et al.* [2014] reported relative permeability measurements with a steady state method. Capillary pressure measurements with the CO_2/water system are rather scarce. Results are reported in *Pentland et al.* [2011], who used the semi permeable disk method [see *Brown*, 1951 or *Christoffersen and Whitson*, 1995]. Drainage capillary pressure curves have also been measured by *Pini et al.* [2012] and *Pini and Benson* [2013] following, with the CO_2/water system, a method developed by *Ramakrishnan and Cappiello* [1991]. An additional way to derive capillary pressure law from core-flooding experiments is through inverse flow modeling and is proposed in *Berg et al.* [2013] or *Wei et al.* [2014].

All these studies have shown the multiphase flow properties to be dependent on the rock itself (wetting character), on the fluids considered, and on the conditions at which they are measured, namely the

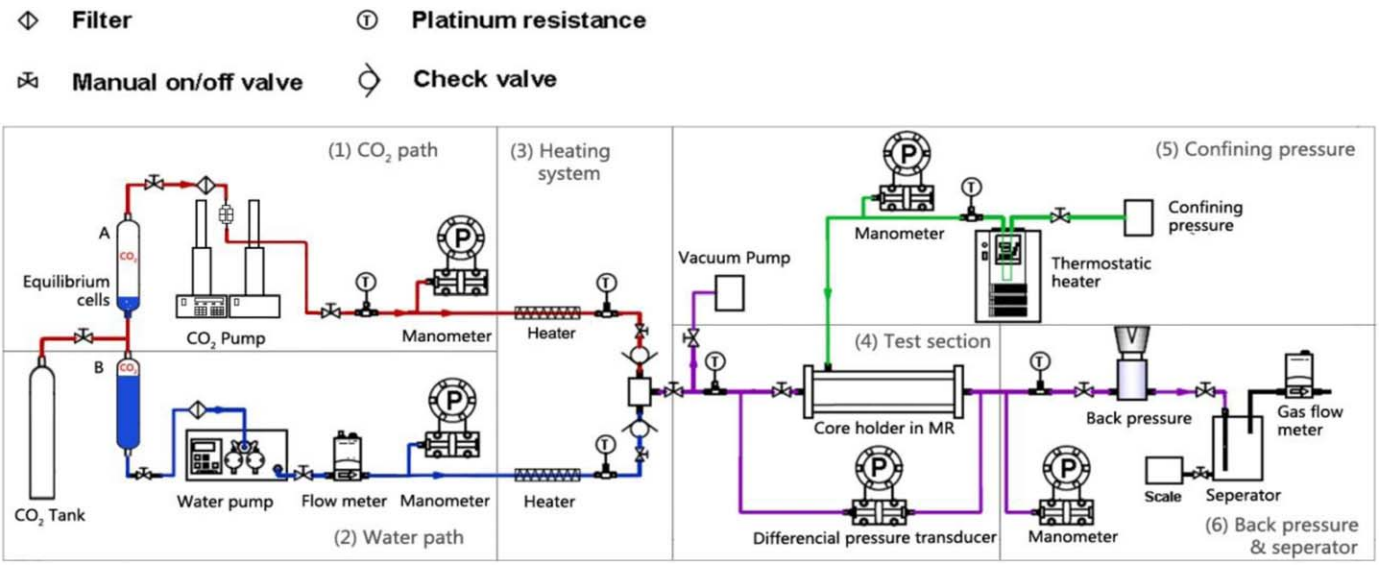

Figure 1. Schematic of the experimental system.

pressure, temperature, and the ratio between the different forces, e.g., between capillary and advective forces [*Krevor et al.*, 2012]. In addition to these parameters linked with the injection protocol, additional challenges might occur during the measurements, due both to the characteristics of the aquifer rock and of the CO_2/water system: in particular, as stated by *Müller* [2011], the presence of minerals reactive to acidic fluid (clay or carbonates) might affect the measurements and the derivation of multiphase flow parameters. The impacts of reactivity on porosity and absolute permeability have been highlighted and measured in previous experimental studies [e.g., *Gouze and Luquot*, 2011; *Lamy-Chappuis et al.*, 2014] as well as its influence on wetting properties modifications [e.g., *Zhu et al.*, 2011]. However, the modifications of capillary pressure and relative permeability properties due to CO_2-induced dissolution and/or precipitation reactions still require quantification efforts.

In this study, we propose new measurements on Triassic sandstone from the Paris Basin, France, following the best practices stemming from the previous works. The characterization of one sample has therefore been done using a two-phase flow core flooding apparatus associated with Magnetic Resonance Imaging at 9 MPa pore pressure and 28°C (CO_2 in liquid state): absolute properties (porosity and water permeability), capillary pressure, relative permeability (with hysteresis between drainage and imbibition), and residual trapping capacities have been assessed. New methodologies for relative permeability and capillary pressure (joint determination of capillary pressure and relative permeability curves using core-flooding technique) and traditional ones (steady-state measurement of relative permeability) have been undertaken. In addition to the extensive data set that has been obtained, we focused our study on the fluid/rock reactivity issues mentioned beforehand. The analyzed sample initially contained carbonates and the experimental protocol has therefore been designed to evaluate their potential impacts on the measurements. Our results suggest that, for a proper characterization of the multiphase flow parameters, the question of mineralogical changes during the measurement procedure needs to be carefully addressed.

2. Materials

2.1. Setup

2.1.1. Core-Flooding Setup

The experimental setup is presented in Figure 1. The rock core is placed horizontally in a core holder within a nuclear magnetic resonance (NMR) system. The materials used in the NMR test section ensure no background NMR signal: the core holder is made in polyether ether ketone (PEEK), the core is wrapped in heat-shrinkable plastic and the confining pressure (set at 11 MPa in our experiments) is ensured by fluorocarbon oil. Two different pumps are used to inject CO_2 (Dual pump Teledyne Isco, Model A500D) and water (SSI/Laballiance Series 1500) at constant rate from one CO_2 tank and one water tank, where the fluids are

equilibrated together. A back pressure valve (Jasco BP-2080-M) is used to ensure a high and constant pressure at the outlet of the core (set at 9 MPa in our experiments). Pressure is measured at the inlet and outlet of the core with two manometers (EJA440A, Span: 6–16MPa, Accuracy: ±0.12 % of Span) and a differential pressure transducer (Honeywell, STD924-F1A00000-MB, 100 kPa, 0.065% full-scale accuracy) allows to measure the differential pressure between the inlet and outlet with more precision. A water mass flow meter (Bronkhorst M12, 0∼200 g/h, 0.5% full-scale accuracy) provides the inlet water mass flow rate while a scale is used to measure the outlet water flow rate. A gas flow meter (Sevenstar Electronics, D07–11CM Mass Flow Meter, 1% full-scale accuracy) serves to measure the outlet CO_2 flow rate after the back pressure valve and the separator. The temperature of the fluids before entering the core and at the outlet is monitored with platinum resistors (Pt100, 0.1 K accuracy). The NMR magnet bodies (one over and one below the core holder) were well temperature-controlled at 32°C, which gave a relatively stable thermal environment at 28°C inside the NMR chamber, where the core holder was placed.

2.1.2. NMR System

In order to quantify the averaged and local saturation during the experiment, nondestructive in situ measuring techniques, as X-ray computed tomography (CT) or nuclear magnetic resonance (NMR) imaging facilities are often associated with regular core flooding apparatus (see for instance *Krevor et al*. [2012] or *Levine et al*. [2014] for CT, *Mitchell et al*. [2013] for NMR). In particular, NMR technique has been used extensively as a reliable and quantitative tool for measuring of water or oil content in saturated or unsaturated porous media in well logging [*Kleinberg and Jackson*, 2001; *Coates et al*., 1999] and core flooding studies [*Timur*, 1969; *Enwere and Archer*, 1992; *Chen et al*., 1993; *Fordham et al*., 1993; *Zhao et al*., 2011].

The system used in this experiment to characterize the fluid content and distribution in the rock sample relies on the proton NMR, i.e., to the response of protons to a magnetic field. The NMR measurements being sensitive to the hydrogen nuclei in the pore water, the rock specific properties like porosity (measurement with NMR of the quantity of water after full saturation), saturation (quantity of water in the pores during the flooding experiments), and pore-size distribution (water distribution in the porous medium) can be estimated.

More precisely, in the presence of the static magnetic field, a magnetic pulses sequence is transmitted (in our case a Carr-Purcell-Meiboom-Gill—CPMG pulse sequence, see *Meiboom and Gill* [1958]) and the NMR relaxation of hydrogen nuclei to their initial state is assessed. The initial signal amplitude recorded at the very beginning of the relaxation is proportional to the number of hydrogen nuclei present in the analyzed sample: if calibrated beforehand with the signal produced by a known volume of fluid, this signal can be converted to a volume of water present inside the sample and therefore to the porosity of the sample or to the saturation within the sample. Two relaxation characteristic times can also be measured during the NMR relaxation: the longitudinal relaxation time (also called T_1) and its distribution as well as the transverse relaxation time (also called T_2) and its distribution. We use here the T_2 time, which for a given porous system is linked to the pore size: in the pores, the relaxation being inversely related to the surface to volume ratio, the smaller pores show shorter T_2 relaxation pores than bigger ones [*Kleinberg et al*., 1994; *Gallegos et al*., 1987; *Roberts et al*., 1995]. The T_2 distribution can thus be seen as a proxy for the pore-size distribution of the sample. All these properties can be measured for the entire rock sample and therefore give averaged value of porosity, saturation, and pore distribution. In our case, these parameters at different points of the rock sample are also of interest for some of the flooding experiments. Therefore to locate the NMR signal within the sample, a gradient in the magnetic field is imposed: the signal frequency emitted by the protons depending on the magnetic field to which it is submitted, it is possible with a varying magnetic field to assess the differences in terms of NMR relaxation at different locations along the core.

In our experiments, the NMR system (Niumag, MesoMR23-060H-I, 21.3 MHz, 0.5 ± 0.05 T) has a magnetic field intensity of 0.5 T and with a magnetic gradient of 0.03 T/m. The NMR signal versus volume of water in the system was initially calibrated: before inserting the core in the core holder, different calibrated volumes of free water (in glass vials) were put inside the core holder ($CuSO_4$ was added to the solution to decrease the relaxation time, which is supposed to be significant for free water). The signal measurements from three calibrated volumes were repeated three times (nine measurement points in total): a linear relationship was derived with a coefficient of determination of 0.9998. Both the signal intensity calibration and the following experiments for whole-core properties are performed with an echo time of TE = 0.42ms. These properties were also measured in several slices along the core (1-D saturation profiles, see e.g., *Olsen et al*. [1996] and

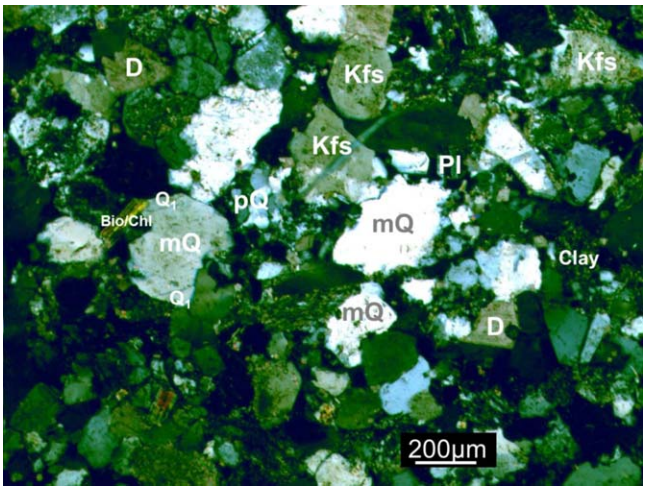

Figure 2. Thin section of the Chaunoy sandstones used in this study (mQ: detrital monocrystalline quartz; pQ: detrital polycritalline quartz; Kfs: K-feldspar; Pl: Plagioclase; Q_1: authigenic quartz; D: dolomite; and Bio/Chl: biotite/chlorite).

Chen et al. [2003]): the thickness of these slices depends on the system properties and has been estimated to 4.9 mm using the following formula [*McRobbie et al*., 2006]: $Thickness = \frac{RFbandwidth}{\gamma * G}$, where *RFbandwidth* is the radiofrequency pulse bandwidth (Hz), γ is the gyromagnetic ratio of hydrogen atom (42.58 MHz/T after *Mohr et al*. [2010]), and *G* is the magnetic gradient of the chosen direction (T/m).

In addition, transversal 2-D images have been collected with the Multi-slice Spin Echo Imaging Sequence [*Chen et al*., 1993; *Fordham et al*., 1993; *Vogt et al*., 2014]. These images only represent a longitudinal slice (4.9 mm) and have therefore been used to have a qualitative picture of the porosity over time.

2.2. Rock and Fluids

The experiments were made on one single cylindrical core (length: 49.5 mm; diameter: 25 mm) from the Chaunoy sandstone formation in the Paris basin, France. The core was taken from 2499.5 m depth. The mineralogical composition of one sample taken close to the studied rock core has been assessed through X-ray diffraction and indicates 69 ± 6.9% of quartz, 15 ± 4.5% of feldspar (11 ± 3.3% of Plagioclase and 4 ± 1.6% of K-Feldspar), 11 ± 3.3% of dolomite, and 5 ± 2% of clay. A thin section micrograph of this sample is also displayed in Figure 2. This sandstone is made of fine-to-medium grains (0.125–0.5 mm) and in terms of mineral composition, the petrographic data, and observations are in line with the studies already performed on Chaunoy formation sand bodies (see e.g., the average petrographic data from the Chaunoy formation in *Worden*, [1998]), which notice the large proportion of quartz and the importance of carbonate cements mostly constituted of dolomite.

Deionized water and carbon dioxide (purity of 99.99%) were used for the core flooding experiments. At the experimental conditions (28°C and 9 MPa), the water density and viscosity are taken to be 1000.2 kg/m^3 and 8.3 × 10^{-4} Pa.s. CO_2 is under the liquid state with a density of 768.4 kg/m^3 and a viscosity of 6.6 × 10^{-4} Pa.s [*Lemmon et al*., 2013]. At those conditions, water evaporates in the CO_2 phase (approximately 1.4 × 10^{-3} in mass fraction, computed with TOUGH2/ECO2N, see [*Pruess et al.,* 1999] and [*Pruess,* 2005]), which might bias the NMR water phase saturation measurement. Considering a conservative water saturation of 25% (in the low range of what is expected to be measured in the experiments), the proportion between the water mass contained in the CO_2 phase over the mass of water molecules contained in the water phase is $\alpha = \frac{0.75*768.4*1.4\cdot10^{-3}}{0.25*1000.2} = 0.32\%$, which is reasonably low to consider negligible the influence of the evaporated water on NMR measurements.

The equilibration between CO_2 and water was done at 5.5 MPa and 20°C (room temperature); the CO_2 solubility in pure water is similar at those conditions than at the experimental conditions in the core-holder (approximately 5.9 × 10^{-2} in mass fraction, computed with TOUGH2/ECO2N).

3. Experimental Protocol

The purpose of the experimental campaign was to assess a large set of properties necessary to characterize the two-phase flow in the porous rock sample with, in addition, a focus on the impacts of a potential reactivity on the two-phase flow properties. Different types of experiments have been performed; their date

Table 1. Experimental Program: Number and Type of the Performed Experiments

Number	Experiment Type
1	Capillary pressure experiment
2	Capillary pressure experiment
3	Relative permeability experiment
4	Relative permeability experiment
5	Residual trapping experiment
6	Residual trapping experiment
7	Capillary pressure experiment
8	Relative permeability experiment

and order of implementation are presented in Table 1. Before each different experimentation, the core porosity and water absolute permeability were measured, respectively, by NMR and by pressure difference monitoring during 100% water flow at 2 or 3 mL/min (ca. 30 pore volumes were injected to ensure the stability of the permeability value). Before starting the experimental campaign, air was evacuated from the core using a vacuum pump, and the system was purged with deaerated water. After each experiments, and before starting a new one, deaerated water was used to flood the core in order to avoid the presence of residual CO_2.

This program has been designed to measure at different times the relative permeability and capillary pressure, in order to see any possible changes in these properties according to the evolution of the absolute properties.

3.1. Capillary Pressure Experiments

The method, originally developed by *Ramakrishnan and Cappiello* [1991], and modified by *Pini et al*. [2012] with the CO_2/water system has been followed. The protocol consists in injecting the nonwetting fluid (expected to be the CO_2 in our case) at constant rate into a core initially saturated with the wetting phase (expected to be water in our case). When the steady state is established, no water is flowing anymore and, as it is the wetting phase, the water phase is expected to be continuous along the core. The water pressure is therefore the same wherever in the core at steady state. If water continuity at the outlet of the core is assumed, the pressure measured at that point is equal to the water pressure in the core. Moreover, the pressure measured before the inlet of the core corresponds to the CO_2 pressure at the core inlet. The differential pressure between the inlet and outlet of the core is therefore equal to the capillary pressure of the core inlet, i.e., corresponding to the core inlet saturation; contrarily to *Ramakrishnan and Cappiello* [1991], who proposed to compute the local saturation at the inlet of the core from the core-average saturation, the inlet saturation is measured as in *Pini et al*. [2012] (in our case, the saturation of the first 4.9 mm is measured with NMR). This protocol is followed for several increasing CO_2 injection rates in order to retrieve several points of the capillary pressure-saturation relationship.

The experiments started by the injection of pure water to ensure a full water saturation of the core and to increase the pressure up to 9 MPa. Then, injection of CO_2-rich water was started during a sufficient time to ensure that the core is fully saturated with this water. The gas flow meter at the end of the setup (after the back pressure valve) allows to know when the CO_2 saturated water reaches this point. After these preparatory stages, the capillary measurements were made by injecting CO_2 at progressive increasing rates. At each rate, after the steady state was reached (noticed by no water flow out of the core and from the stabilization of a constant differential pressure), the saturation of the inlet of the core was measured with the NMR system and the inlet-outlet differential pressure was recorded. The pressure drop corresponds to the capillary pressure at the saturation of the inlet of the core.

The CO_2 volumetric flow rates were comprised between 0.1 and 25 mL/min corresponding to capillary numbers N_c between 2×10^{-6} and 8×10^{-9}—considered as $N_c = \frac{v \cdot \mu}{\sigma}$, where v, μ, σ are, respectively, the fluids Darcy velocity in $m.s^{-1}$, the CO_2 viscosity in Pa.s, and the interfacial tension for the CO_2/water pair in $N.m^{-1}$ estimated after *Georgiadis et al. [2010]* at 29.97 $mN.m^{-1}$ (an average value was computed from the 8 MPa/25°C value—30.28 $mN.m^{-1}$—and the 10 MPa/25°C value—29.66 $mN.m^{-1}$). The highest capillary number values (2×10^{-6}) is much below the threshold for the mobilization of the irreducible wetting phase saturation reported in *Dombrowski and Brownell* [1954] (10^{-3}), ensuring a capillary-dominated regime during our experiments.

3.2. Relative Permeability Experiments

Steady state relative permeability measurements were performed to derive the relationship between the effective permeability to CO_2 and water according to the pore saturation. Similarly to the capillary pressure experiments, the core was saturated with pure water and then with CO_2-saturated water at 9 MPa. Then,

CO_2 and water were injected simultaneously at a constant total volumetric flow rate (2 mL/min) and at several CO_2-fractional flows (nine different fractional flows from 0.06 to 0.99). For each fractional flow, the pressure drop between the core inlet and outlet was recorded after steady state was established (noticed from the stabilization of a constant differential pressure and of the NMR signal). Then the core was scanned with the NMR system to retrieve the average saturation in the core (scans were performed regularly until a stable value was reached). Finally, knowing the CO_2 and water flow rates for each fractional flow, the relative permeability to CO_2 and to water were computed using the two-phase flow Darcy's law: $k_{r,i}=q_i\frac{\mu_i L}{Ak\Delta P}$, $i=CO_2$ *or water*, with q, L, A, and ΔP being, respectively, the flow rate, the length and cross-sectional area of the core, and the pressure drop between the core inlet and outlet. Note that this equation presupposes a constant saturation and a constant capillary pressure along the core. Therefore, the capillary end effects and heterogeneities might impact the measurements (the capillary end effects are further discussed in the results section). Measurements were performed both for drainage and for the first imbibition during experiment 4. For this experiment, after increasing progressively the fractional flow up to 0.99, it was decreased down to 0.05 (eight different fractional flows). The experimental conditions corresponded to a capillary number of 1.eight 7×10^{-7} (computed for CO_2 properties, i.e., for the highest fractional flow at the end of the drainage), which is in the range of representative values for CO_2 geological storage injection conditions [*Krevor et al*., 2012].

In addition to the data for relative permeability to CO_2 and water for drainage and imbibition gathered from the steady state technique, data for drainage relative permeability to CO_2 have been derived from the capillary pressure experiments, as proposed in *Ramakrishnan and Cappiello* [1991] and modified in *Pini and Benson* [2013] to account for a different pressure condition at the outlet of the core. The principle is briefly presented here: The local Darcy's equation during the capillary test (drainage test with 100% CO_2 injection) at steady state (i.e., no water is flowing anymore) is:

$$q=\frac{Akk_{r,CO_2}}{\mu_{CO_2}}\cdot\frac{dP_c}{dx}, \tag{1}$$

where q is the volumetric flow rate, $k_{r,CO2}$ is the relative permeability to CO_2, and x the position variable along the core. Since saturation is varying along the core, the capillary pressure and relative permeability to CO_2 are changing as well. However, since the differential pressure between the inlet and outlet of the core is very small compared to the pressures both at the inlet and the outlet, the volumetric flow rate and the viscosity are assumed constant along the core (this has to be validated when conducting the experiments), which gives:

$$q_{inj}L=\frac{Ak}{\mu_{CO_2}}\int_{\Delta P_{c,x=0}}^{P_{c,x=L}}k_{r,CO_2}(P_{c,x})dP_{c,x}, \tag{2}$$

$P_{c,x=0}$ corresponding to the pressure measured during the capillary pressure tests and $P_{c,x=L}$ to the capillary pressure at the outlet of the core considered as the entry capillary pressure of the rock. We note $\Delta P_{c,x}=P_{c,x}-P_{c,x=L}$ the capillary pressure difference between one location along the core and the core outlet. The previous equation is changed into:

$$q_{inj}L=\frac{Ak}{\mu_{CO_2}}\int_{\Delta P_{c,x=0}}^{0}k_{r,CO_2}(\Delta P_{c,x})d\Delta P_{c,x}. \tag{3}$$

The differentiation of this equation relatively to $\Delta P_{c,x=0}$ gives, if a homogeneous relative permeability law is assumed to be followed along the core:

$$\frac{dq_{inj}}{d\Delta P_{c,x=0}}=\frac{Ak}{\mu_{CO_2}L}\cdot k_{r,CO_2}(\Delta P_{c,x=0}) \tag{4}$$

This equation means that the relative permeability of CO_2 can be found knowing the relationship between the injection rate and the pressure measured during the capillary pressure experiments.

With this approach, the relative permeability is obtained at the core inlet saturation during 100% CO_2 flow at higher rates than those used with the steady state method: this approach is therefore used to retrieve

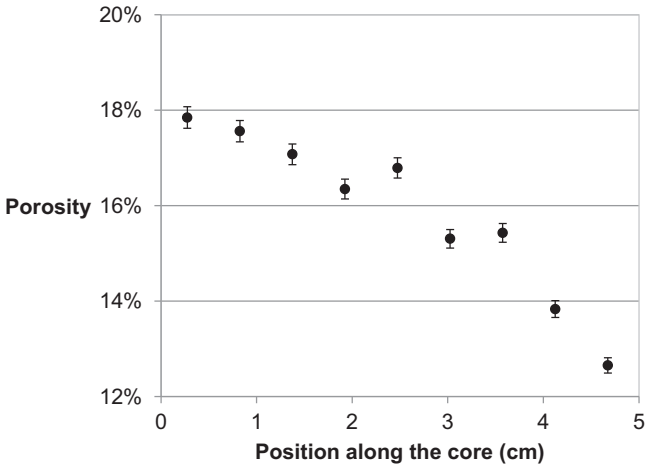

Figure 3. Average porosity profile along the core. The dots represent porosity average in a 5 mm thick slice. The core flooding is performed in the 0—5 cm direction.

relative permeability values for high CO_2 saturation for completing the steady state results but it only provides CO_2 relative permeability values during the drainage stage.

3.3. Residual Trapping Experiment

The last type of flow experiments with the CO_2/water was performed to assess the residual trapping properties of the core. The fraction of CO_2 that is residually trapped after imbibition has been shown to be dependent on the initial CO_2 saturation before the imbibition starts [*Krevor et al*. 2012, *Akbarabadi et al*. 2013]. One rapid way to estimate this dependence is to inject 100% CO_2 until a given saturation distribution occurs in the core and to follow with an imbibition with 100% CO_2-saturated water in order to observe the new saturation distribution along the core. The experiments started with the injection of pure water followed by the NMR imagining of the core in order to have a reference to calculate the average saturation in several slices of the core. The core was then saturated with CO_2-saturated water before starting the 100% CO_2 injection at 1 mL/min. After steady state was established, the core was imaged to retrieve the saturation distribution along the core after drainage. The CO_2 injection was then stopped and CO_2-saturated water was injected (same rate then for CO_2) until steady state, when the core was imaged with NMR again. The saturation distribution at steady state corresponds to the residual saturation after imbibition. This experiment was used to derive the initial versus residual CO_2 relationship but the saturation after drainage can also give insight into the longitudinal rock heterogeneities.

4. Results: Two-Phase Flow Characterization

4.1. Porosity and Absolute Water Permeability Measurements

The petrophysical properties of the core have been measured before experiment 1 and show an average porosity of 15.8% (pore volume of 3.8 mL measured through NMR) and an initial water permeability of 85 mD. Even though it was not visually detectable, a heterogeneity trend was observed when measuring the porosity in different slices of the core with NMR gradient, with a progressive decrease in porosity along the core (see Figure 3).

In addition to that initial characterization, porosity and absolute water permeability were measured prior to each experiment and the results of these measurements are provided on Figure 4. Error bars indicate the minimum and the maximum values of both parameters during the measurements. The uncertainty is generally low and a global increase of both parameters can be noticed (an unexplained high uncertainty regarding the porosity measurement can be noted for experiment 2 but it does not impact the general porosity evolution trend). Interestingly, the increase is less obvious at the beginning of the experimental campaign when capillary pressure experiments were performed and seems to have been enhanced by the relative permeability experiments. This apparent correlation between the absolute flow properties and the type of experiments performed is further discussed in the last section of this paper.

4.2. Capillary Pressure Experiment

Capillary pressure has been assessed at three different times (experiment 1, 2, and 7). For each experiment and for each rate, the saturation and the pressure drop recorded are recalled in supporting information. They are plotted on Figure 5 with, in addition, the best fit Brooks and Corey curves [*Brooks and Corey*, 1964]

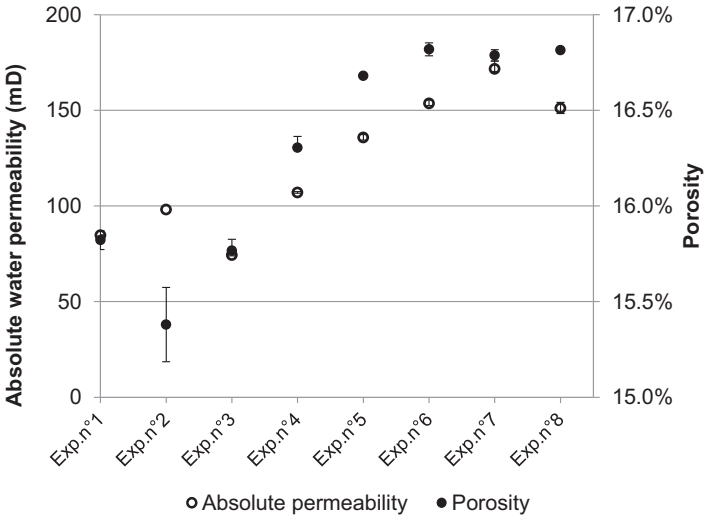

Figure 4. Evolution of the sample porosity and absolute water permeability over time.

and error bars indicating the minimum and the maximum values of the pressure drop measured during the measurements.

One particularity of the measurements results is the impossibility, even for very small flow rates, to gather data for high water saturation. This is explained by the fact that, in our experiments, the control is on the flow rate rather than on the pressure drop. The relatively low absolute water permeability of the rock sample gives rise to a relatively high pressure drop even for small flow rates. In addition, the relatively low capillary pressure associated to this pressure drop causes a high saturation at the core inlet. However, the saturation range with no data corresponds, for this specific rock, to small capillary pressure values, which are not of first importance in terms of use of this data set for large-scale modeling of CO_2 storage operations (the entry pressure, even if it not precisely known, is very low—inferior to 6 kPa—and would be overcome during the pressure induced by such operations); the end of the small capillary pressure plateau and the sharp increase observed for low water saturation values are the most important curve features and are well-captured by the experiments. This behavior, i.e., a small evolution of capillary pressure values for a large saturation range followed by a sharp increase, indicates a narrow pore-size distribution. Regarding the evolution of the capillary pressure over the experiments, an apparent decrease of the capillary pressure between experiments 1, 2, and 7 can be suspected. It should be noted that, during the capillary pressure measurements, only the pressure variations (and not the saturation ones) have been measured. Nevertheless, the comparison between the capillary pressure plateau of the three experiments is more influenced by pressure than by saturation uncertainties and tends to confirm a lower capillary pressure for experiment 7.

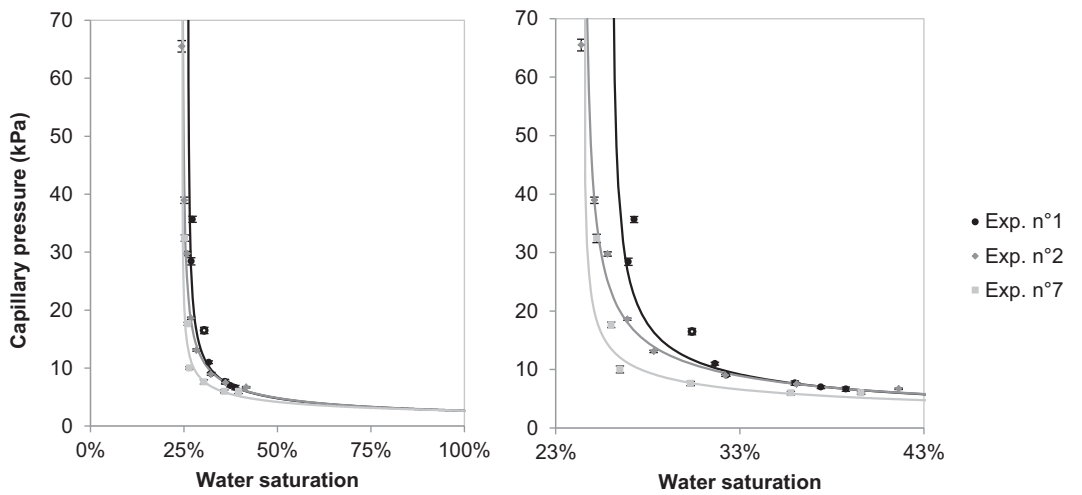

Figure 5. Capillary pressure results (left: entire saturation range, right: zoom); solid lines represent general trends estimated with Brooks and Corey curves (the empty symbol was not considered in the fitting procedure as it did not line up with the general trend).

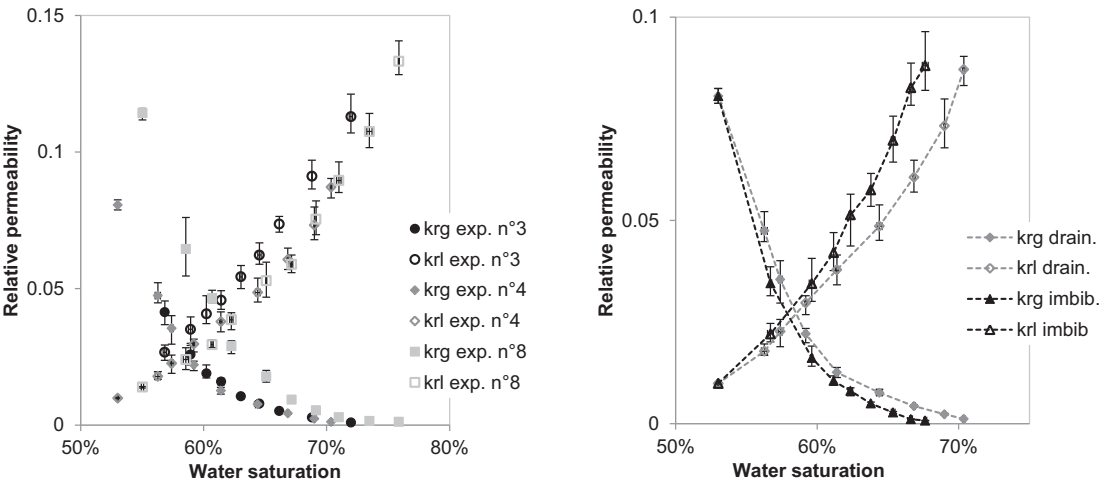

Figure 6. Steady state relative permeability results: (left) drainage for experiment 3, 4, and 8/(right) Drainage and first imbibition for experiment 4.

4.3. Relative Permeability Experiment

Steady state relative permeability results (for experiments 3, 4, and 8, with drainage and imbibition for experiment 4) are shown in Figure 6 as a function of the water saturation and the data are recalled in supporting information; error bars indicate the minimum and the maximum values of relative permeability (pressure drop) and saturation measurements (after stability was noticed, two NMR scans were performed for each of the 36 saturation measurements).

The differences during the three experiments for the drainage process seem to show a progressive increase in CO_2 relative permeability and a decrease in water relative permeability, even though the former is much more noticeable. The differences in CO_2 relative permeability have a visible impact on the fractional flow as a function of the saturation, as shown in Figure 7: at a given water saturation, the CO_2 fractional flow appears to be higher during experiment 8.

The hysteresis effects between the drainage and the first imbibition are not significant notably because of the small range of saturation scanned during the steady state experiment. Nevertheless, the changes observed between the two processes are similar to the observations made in previous studies [e.g., *Akbarabadi et al.*, 2013]: during imbibition, a lower CO_2 relative permeability and a higher water relative permeability are observed compared to drainage.

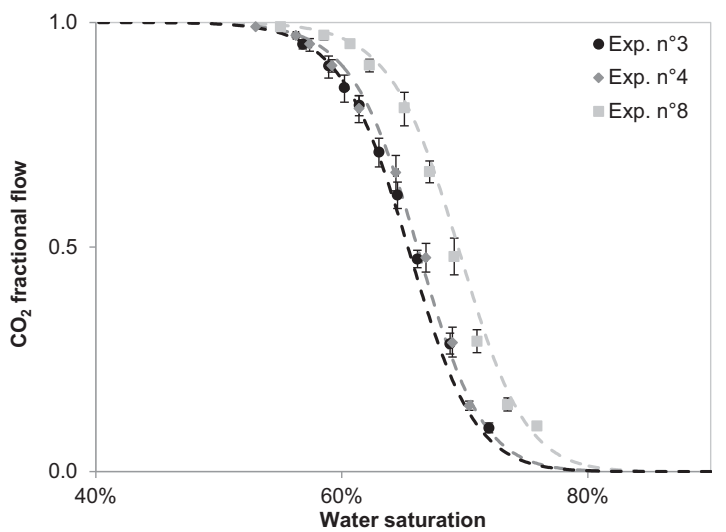

Figure 7. CO_2 fractional flow observed during experiments 3, 4, and 8. The dashed lines represent the fractional flow computed after the fitting of the CO_2 and water steady state relative permeability measurements with *Lenhard and Parker* model [1987].

It can be noted that for each of the measurements, the saturation range that was scanned is rather small; especially, even for CO_2 fractional flow of 0.99, it was not possible to decrease the water saturation below 50%. This phenomenon of low nonwetting phase saturation end-point has been explained to be due to heterogeneities by *Berg et al.* [2013] or to capillary end-effects by *Huang and Honarpour* [1998], but also to the capillary pressure possibly

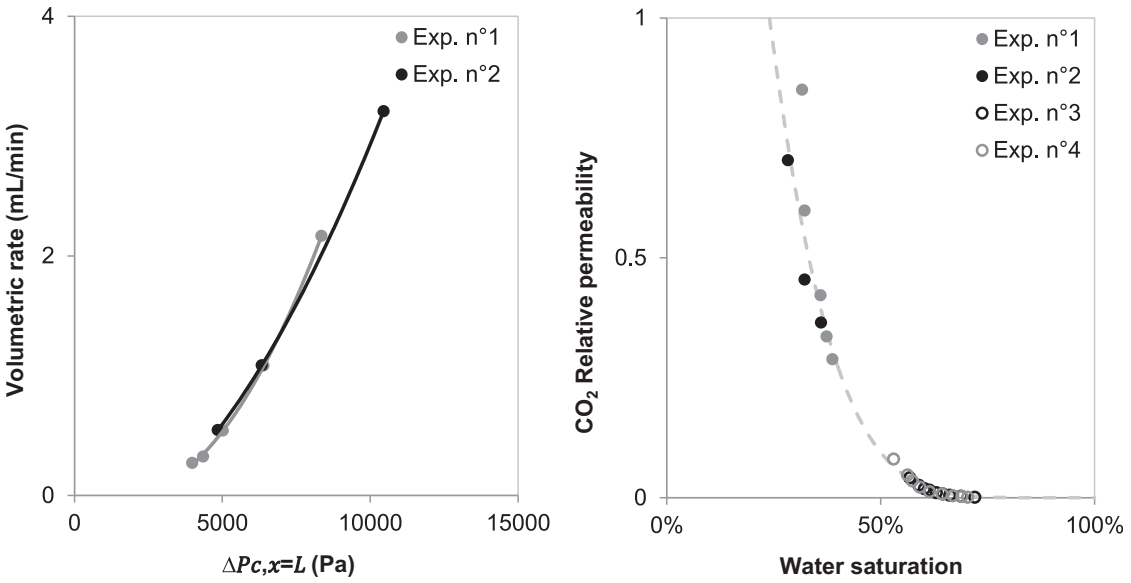

Figure 8. Determination of the CO_2 relative permeability during drainage from the capillary pressure experiments: (right) relationship between the volumetric rate and the capillary pressure difference during experiments 1 and 2; (left) comparison between the results from the capillary pressure experiments 1 and 2 and the steady state relative permeability measurements from experiments 3 and 4. The dashed line represents the fitting with *Lenhard and Parker* model [1987].

reached by the system by *Krevor et al*. [2012]. The last reason seems to occur here since an average saturation of 46% has been reported during experiment no 1 with a 100% CO_2 flow rate of 2 mL/min: it is therefore logical to observe lower average saturations during relative permeability experiments when the same rate was used with a CO_2:water ratio always below 99%. However, the sample used was shown not to be completely homogeneous (porosity decrease) and therefore the first reason (heterogeneity) cannot be entirely neglected. The capillary end effects might also have impacted the results of relative permeability measurements since a flat saturation profile is required to compute this value. To assess the relevance of this phenomenon, a 1-D simulation of the steady state relative permeability experiments was performed with TOUGH2 [*Pruess et al.,* 1999] and the ECO2N [*Pruess,* 2005] module (100 cells). The porosity and permeability of experiment 3 are considered with the relative permeability and capillary pressure laws used to fit the data measured that very day. The highest CO_2-fractional flow (0.95), i.e., leading to the highest capillary end effects has been simulated. According to the simulations, the capillary end effects are very low: 4.85 cm of the core (the total length is 4.95 cm) have a CO_2 saturation superior or equal to 95% of the maximum saturation in the core.

To go above the saturation range limitations of the steady state method, we use the capillary pressure measurements (where higher CO_2 flow rates and therefore higher capillary pressures, and higher CO_2 saturations were reached) as proposed by *Pini and Benson* [2013] and described in section 3.2. The maximum differential pressure in the core (65.5 kPa) induces a 0.2 % density change and a 0.4 % viscosity change between the two core extremities: this validates, in our case, the constant density and viscosity approximation that has been made in section 3.2 calculations. This method relies on the estimation of the relationship between the injection rate and the pressure measured during the capillary pressure experiments, and more precisely on the derivative. For sake of precision, the fitting (second-order polynomial regression) of this relationship has been done on the rates comprised between 0.5 mL/min and 4 mL/min, which are considered as the most accurate rates. The regression and the results from capillary pressure experiments 1 and 2 are displayed on Figure 8. They are compared to the steady state relative permeability results from experiments 3 and 4 in order to lower the impacts of rock property changes over time, and fitted with *Lenhard and Parker*'s model [1987]. The comparison shows a fair complementarity between the two kinds of measurements allowing to have an estimation of the CO_2 relative permeability for a higher range of saturation.

4.4. Residual Trapping Experiment

Residual trapping capacities of the rock sample were assessed at two different times (experiments 5 and 6). The saturation was estimated after the end of drainage (initial saturation prior to imbibition) and after the end of

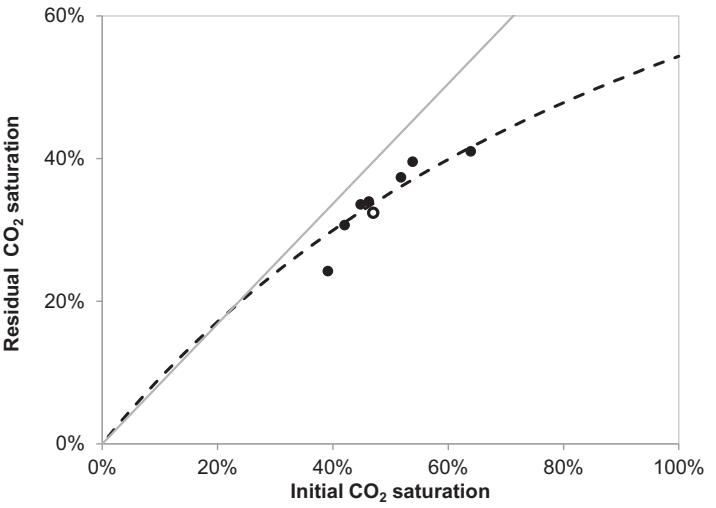

Figure 9. Residual saturation versus intial saturation (prior to imbibition). Filled circles correspond to experiments 5 and 6 results. Empty circle corresponds to the result of experiment 4. The dashed line represents Land model with C = 0.84. The gray line is a 1:1 line.

imbibition (residual saturation) in five different slices of the rock samples. The relationship between the initial and residual saturation is shown on Figure 9. The core-averaged saturation after drainage and imbibition of experiment 4 is also added. The relationship appears to be monotonic, which suggest a water-wet character of the rock [*Spiteri et al*., 2008]. Also, the results respect fairly the Land model [*Land*, 1968], adapted to water-wet systems, where the initial CO_2 saturation before imbibition ($S_{CO_2,ini}$) is related to the residual CO_2 saturation ($S_{CO_2,res}$) by $S_{CO2,res} = \frac{S_{CO2,ini}}{1+CS_{CO2,ini}}$, C being called the Land coefficient and found to be equal to 0.84 in our case. The trapping efficiency has been found to vary between 62 and 75%. Comparing these data with those reported in literature for different sandstones, the Chaunoy sandstone seems to trap a relatively large quantity of CO_2: the Land coefficient for Berea, Paaratte, Mt. Simon, and Tuscaloosa sandstones were, respectively, 1, 1.3, 2.1, and 1.7 in *Krevor et al*. [2012] and *Akbrabadi and Pini* [2013] observed a trapping efficiency varying between 49 and 61% for Berea sandstone and between 64 and 78% for Nugget sandstone.

5. Discussion: Implication of Changes Over Time on the Flow Parameters

As stated by *Müller* [2011], the acidic environment due to CO_2 dissolution in water/brine may have an influence on the porous medium mineralogy, and can potentially impact the absolute or/and the two-phase properties of the medium. As described previously, the porous medium used for this study, even though mainly constituted of quartz, initially contained a nonnegligible part of carbonate cement (11%, see section 2.2), which has been shown to dissolve rapidly in an acidic solution. Moreover, the experimental protocol has been designed to measure the flow properties at several times during the experimental campaign, as explained in section 3. In this section, we propose to discuss the impacts of mineralogical changes on flow properties and to this aim, we first provide observations on the mineralogy and pore structure of the core over time and then discuss how these modifications could be linked with the results obtained in section 4 for porosity, water permeability, capillary pressure, and relative permeability.

At the end of the experimental campaign, the composition of two slices of the core (one close to the inlet—8 mm—and one close to the outlet—8 mm) has been assessed. The main change that has been observed with X-ray diffraction is a diminution of the carbonate content which seems to have decreased more at the core inlet than at the core outlet ($3 \pm 1.2\%$ and $6 \pm 1.8\%$ of total carbonate, respectively, close to the inlet and close to the outlet of the core compared to $11 \pm 3.3\%$ at the beginning of the experiments), while the other minerals have remained constant. The observation of two thin sections (Figure 10) did not show clear evidence of the presence of carbonates. These mineralogical observations have been completed by the qualitative analysis of the magnetic resonance imaging of the core performed prior to any experiments and after the experimental campaign: MR images have been taken before experiment 1 and after experiment 8, with the rock sample fully saturated with pure water: the intensity of the two images was therefore related to the quantity of water. These images have been normalized and subtracted. Figure 11 shows that the difference is mostly positive and much higher than the difference in background noise which is very close to zero. This indicates that the porous volume is higher after the experiment than before (confirmation of the global increase of porosity described in section 4.1), and that the porosity increase occurs mostly at the core inlet with a progressive diminution of the increase along the core length. These

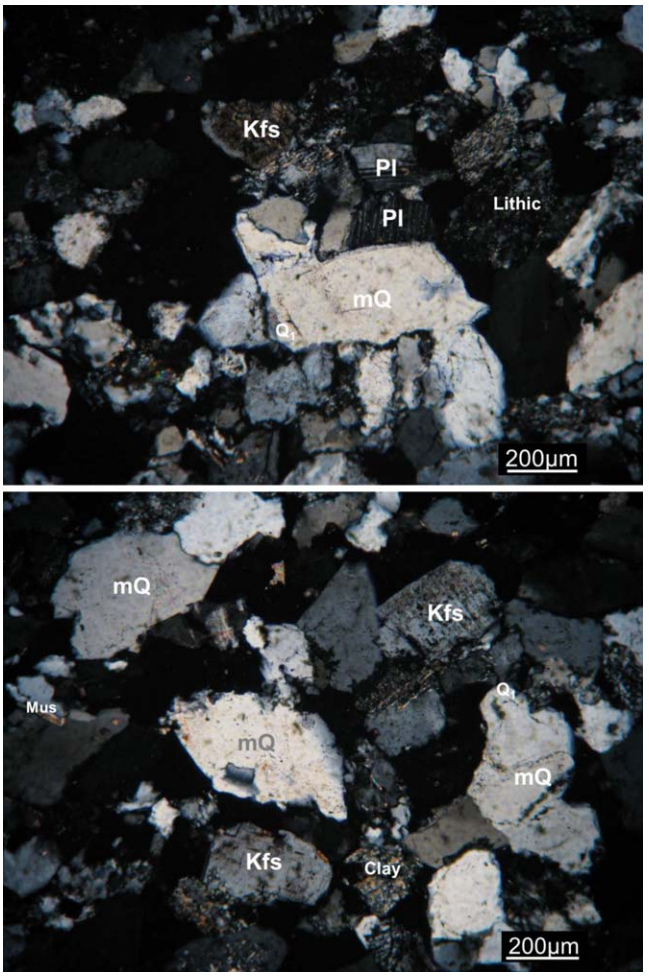

Figure 10. Thin section from two parts of the core after the experimental campaign: (top) close to the inlet of the core; (bottom) close to the outlet (mQ: detrital monocrystalline quartz; Kfs: K-feldspar; Pl: Plagioclase; Lithic: quartzose lithic fragment; Q_1: authigenic quartz; and Mus: muscovite).

observations seem to be in line with the evolution of a carbonate dissolution front through the core, starting at the core inlet where new carbonated water enters the porous medium. Figure 11 also shows that, given the noise in the NMR images, no (or very few) increase in pore volume (precipitation) is observed (the difference of signal is positive almost everywhere). In addition, the modifications in pore structure were also observed over time, through the T_2 time distribution. The T_2 distribution of the whole core was inverted from the NMR signals recorded after each different type of experiments (capillary pressure, relative permeability, and residual trapping). We recall that these curves represent the cumulative population of each individual T_2 times, which are longer for the larger pores of the core. The conversion of the T_2 time into a quantitative pore-size distribution is, however, dependent on the surface relaxivity and of the pore geometry (*Kleinberg et al*. [1994]), and therefore has not been performed in this study. The T_2 distribution is presented on Figure 12. It shows an increase in the cumulative signal distribution for a significant range of T_2 times and notably confirms the pore volume increase over time (the total cumulative signal is higher after the experiments). More interestingly, the changes seem to have occurred more significantly during the relative permeability experiments when new water with dissolved CO_2 was flushed in the sample during a long time, compared to capillary pressure experiments where mostly CO_2 phase was flowing leading to a less aggressive chemical environment. This would also indicate that the flow of deionized water performed before and after each experiment notably to measure the absolute water permeability and to saturate the core did not lead to major chemical reactions. To confirm these observations, a 1-D reactive transport model was developed using PHREEQC v3 calculation code [*Parkhurst and Appelo*, 2013] comparing the effect of a 1 h flow of deionized water with that of deionized water with dissolved CO_2 at temperature, pressure, and rate conditions equal to those of relative permeability experiments (28°C, 9 MPa, and 2 mL/min). Without CO_2, the average dolomite content decreases from 10.27% (initial content) to 10.25%, while with CO_2, it decreases to 7.69% (i.e., a relative decrease of, respectively, 0.2 % and 25%). Even if the computation is likely to overestimate the changes (all the dolomite content is in contact with the flowing water and the reaction is considered instantaneous), it shows that the consequences of deionized water flow are low compared to those of CO_2-dissolved water flow. Moreover, the simulations report a decrease occurring preferentially at the core inlet.

Porosity and absolute water permeability were measured prior to each experiment; the results of these measurements are provided on Figure 4. A global increase of both parameters has been observed, which is

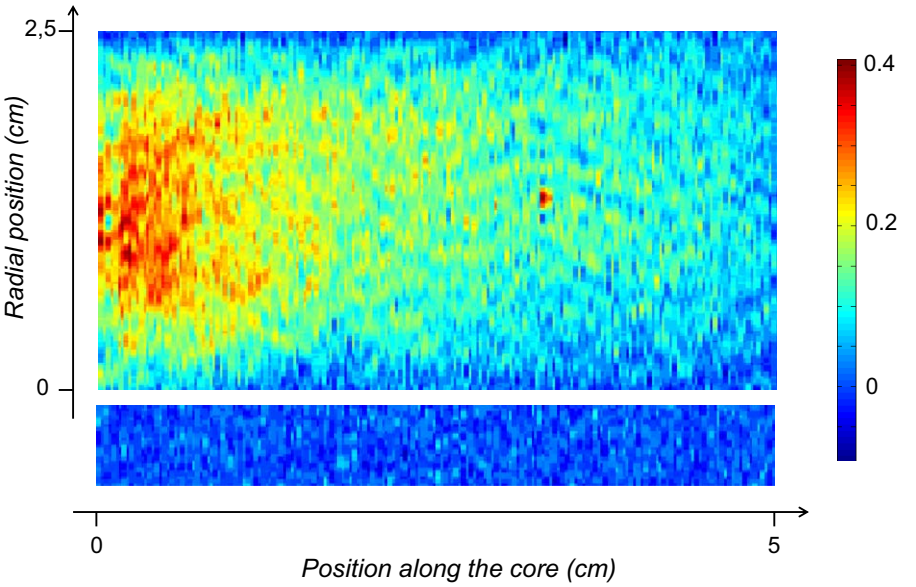

Figure 11. Difference of magnetic resonnance images of the longitudinal cross section between the intial core and the core after experiment 8 (the initial magnetic resonnance image signal was normalized between 0 and 1). The top image corresponds to the core longitudinal cross section while the bottom one provides the difference of NMR signal outside of the core to assess the background noise level.

in accordance to the pore volume increase volume that has been assessed. The correlation between the absolute flow properties changes and the type of experiments is also visible: the increase is less obvious at the beginning of the experimental campaign, while it becomes stronger when relative permeability experiments started. The impact of small changes of porosity appears to have significant consequences on water permeability with an increase of approximately 6 % in porosity and 80 % in permeability at the end of the experiments compared to the beginning. This does not satisfy the empirical porosity-permeability correlation of Kozeny-Carman [*Bear*, 1988]: $k \propto \varphi^3/(1-\varphi)^2$. Using this equation, the water permeability obtained at the end of the experiments would indeed be estimated to be approximately 20 % higher with the observed porosity increase. The same observations have recently been made by *Lamy-Chappuis et al.* [2014], who explained this phenomenon by an increase in connectivity (i.e., arrangement of pore connections) and/or a reduction in tortuosity (i.e., relative flow paths length). In our case, the dissolution of carbonate cements seems to have modified different range of the pore-size distribution (small and larger pores, *cf.* the T_2 distribution curve on Figure 12). Therefore different explanations (possibly combined) may be given for the large increase of water permeability such as pore-

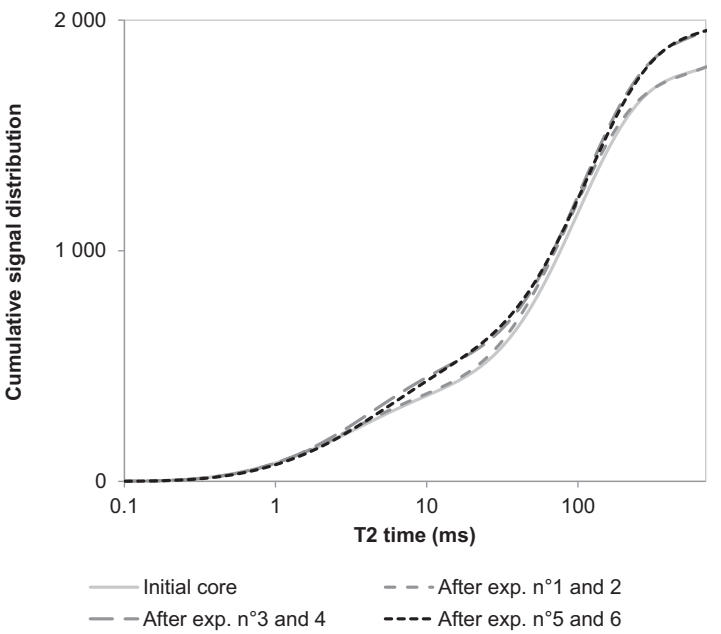

Figure 12. Cumulative T_2 distribution in the whole core measured prior to any experments and after the different experiment types (the signal for $T_2 > 800$ ms is not displayed as it is likely to be influenced by the small lines and the disks outside of the core). The total cumulative signal represents the NMR signal from the water content present in the porous medium.

throat dissolution or the dissolution of larger grains opening new flowing paths, which could have affected the connectivity or the tortuosity.

Figure 5 shows the differences between the different measurements of capillary pressure. Even though some differences can be seen for the highest capillary pressure values (suspected to be due to measurement imprecisions during the sharp capillary pressure increase), the capillary pressure is rather stable for capillary pressure below 15 kPa between experiments 1 and 2. The capillary pressure has, however, been found to be lower during experiment 7. This is in line with the previous section, since it has been shown that the first slice of the core—where the capillary measurements have been performed—is not much impacted by mineralogical reactions between experiments 1 and 2 but is subject to modifications before experiment 7. The relevance of this change in capillary pressure can be in a first approach investigated by considering the J-function proposed by *Leverett* [1941], originally defined as $J=\frac{Pc}{\sigma}\sqrt{\frac{k}{\varphi}}$, which has been developed to correlate capillary pressure curves to rock properties. With the changes in porosity and water permeability for the whole core observed between experiments 2 and 7, $\frac{Pc,exp7}{Pc,exp2}<1$, which appears to be consistent with the capillary pressure observations. According to *Anderson* [1987a], no simple relationship can be derived between capillary pressure and wettability. Even though some authors have observed an increase in capillary pressure for decreasing contact angles [e.g., *Ishakoglu and Baytas*, 2005], some others concluded that this evolution is not visible for all contact angles range, especially for drainage capillary pressure curves [e.g., *Morrow*, 1976]. Therefore, the results obtained for capillary pressure cannot be directly used to discuss potential wettability evolution of the rock sample.

The differences in terms of relative permeability to CO_2 and water (displayed on Figure 6) seem to show, for the same experimental conditions, a progressive increase in CO_2 relative permeability and, to a lower extent, a decrease in water relative permeability. *Morgan and Gordon* [1970] studied experimentally the influence of pore geometry on water-oil relative permeability and found that, in general, rocks with large pores allow high relative permeability end points. *Ghassemi and Pak* [2011] also captured this phenomenon through a numerical study and reported that increasing the specific surface area of the porous medium (i.e., diminishing the pores size) does not influence much the relative permeability to the wetting phase but may reduce significantly the relative permeability to the non-wetting fluid. Our observations, similar to these results, could therefore be linked with the size increase of some pores because of the carbonate dissolution. However, relative permeability has also been shown to be related to rock wettability: according to the reviews performed by *Anderson* [1987b] and *Krevor et al*. [2012], who studied these effects, an increase of the relative permeability to CO_2 associated with a decrease of the relative permeability to water could indicate an increase of the rock water-wettability. Moreover, *Espinoza and Santamarina* [2010] reported contact angle results for CO_2/deionized water/mineral systems (up to 10 MPa and 25°C) both for quartz and calcite minerals: they show notably that quartz minerals have a higher wetting character (lower wetting contact angle) than carbonate minerals (calcite). Thus, the increase during the experimental campaign of the proportion in quartz compared to carbonates because of mineral dissolution could be an explanation to the wettability increase and consequently an additional explanation to the induced relative permeability evolution that was observed.

6. Conclusions

A rock sample from a Triassic sandstone rock located in the Paris Basin (Chaunoy sandstone) has been characterized using a set of core-flooding methods. The purpose of this work was to describe the major absolute and two phase flow properties (CO_2/water system) to be upscaled and used in large-scale plume evolution modeling tools. Nuclear magnetic resonance was used to characterize the pore structure and the water content (i.e., fluid saturation) in the rock during the flooding experiments. In addition to a characterization of the absolute properties of the rock, data were collected with the same core-flooding system on capillary pressure, relative permeability (for drainage and imbibition stages), and residual trapping capacities of the rock. They show classical properties for a well-sorted water-wet sandstone.

The sandstone sample being constituted of a nonnegligible proportion of carbonates, the experimental protocol was designed to assess the impact of potential mineral changes. The magnetic resonance scanning and mineralogical observations indicate a dissolution of carbonates along the experiments. Some modifications of the absolute parameters occurred, with an increase in porosity and water permeability.

Interestingly, we also observed some changes in the two-phase flow parameters correlated with the absolute properties changes, indicating mostly a decrease of capillary pressure and an increase of the CO_2 relative permeability. The changes in absolute and two-phase flow properties are coherent with the pore structure modification induced by the carbonates dissolution. The changes in relative permeability could also be linked to wettability modifications, which could be attributed to the dissolution of the less-wetting minerals. These results need to be compared to additional studies on the impacts of mineralogical reactions on rock flowing properties in a CO_2/water system, especially in carbonate-rich formation that can be investigated for storage operations. This can indeed be an important phenomenon to account for regarding the validity of the laboratory measurements of these properties, and regarding the input parameters to consider in the flow-modeling of in situ operations.

Acknowledgments

The data for this paper are available in supporting information or by contacting the corresponding author. This research has been supported by the National Natural Science Foundation of China (51376104), Science Fund for Creative Research Groups of the National Natural Science Foundation of China (51321002), and by Carnot funding. We thank the SALTCO project cofunded by the French Environment and Energy Management Agency (ADEME) and BRGM (contract 1094C003) for providing the cores used and the Tsinghua University Initiative Scientific Research Program. The manuscript was significantly improved thanks to the helpful reviewers' comments.

References

Akbarabadi, M., and M. Piri (2013), Relative permeability hysteresis and capillary trapping characteristics of supercritical CO_2/brine systems: an experimental study at reservoir conditions, *Adv. Water Resour.*, *52*, 190–206.

Anderson W. (1987a), Wettability literature survey: Part 4: Effects of wettability on capillary pressure, *J. Petrol. Technol.*, *39*(10), 1283–1300.

Anderson W. (1987b), Wettability literature survey: Part 5: Effects of wettability on relative permeability, *J. Petrol. Technol.*, *39*(10), 1453–1458.

Bachu, S., and B. Bennion (2008), Effects of in-situ conditions on relative permeability characteristics of CO_2-brine systems, *Environ. Geol.*, *54*, 1707–1722.

Bear J. (1988), Dynamics of Fluids in Porous Media, 764 pp., Dover, Mineola, N. Y.

Bennion, B., and S. Bachu (2005), Relative permeability characteristics for CO_2 displacing water in a variety of potential sequestration zones in the Western Canada Sedimentary Basin, paper SPE 95547 presented at the 2005 SPE Technical Conference and Exhibition, 15 p., Dallas, Tex., 9–12 Oct.

Bennion, D. B., and S. Bachu (2008), Drainage and imbibition relative permeability relationships for supercritical CO_2/brine and H2S/brine systems in intergranular sandstone, carbonate, shale, and anhydrite rocks, *SPE Reservoir Eval. Eng.*, *11*(3), 487–496.

Bennion, D. B., and S. Bachu (2010), Drainage and imbibition CO_2/brine relative permeability curves at reservoir conditions for carbonate formations, paper SPE 134028Annual Technical Conference and Exhibition, 1–18 pp., Soc. of Pet. Eng., Florence, Italy.

Berg, S., S. Oedai, and H. Ott (2013), Displacement and mass transfer between saturated and unsaturated CO_2-brine systems in sandstone, *Int. J. Greenh. Gas Control*, *12*, 478–492.

Brooks, R. H., and A. T. Corey (1964), Hydraulic properties of porous media, *Hydrol. Pap.*, *3*, pp. 1–27, Colo. State Univ., Fort Collins, Colo.

Brooks, R. H., and A. T. Corey (1966), Properties of porous media affecting fluid flow, *J. Irrig. Drain. Div., Am. Soc. Civ. Eng.*, *92*(IR2), 61–88.

Brown, H. W. (1951), Capillary pressure investigations, *Pet. Trans. AIME*, *192*, 67–74.

Chang, C., Q. Zhou, L. Xia, X. Li, and Q. Yu (2013), Dynamic displacement and non-equilibrium dissolution of supercritical CO2 in low-permeability sandstone: An experimental study, *Int. J. Greenh. Gas Control*, *14*, 1–14.

Chen, S., F. Qin, K. H. Kim, and A. T. Watson (1993), NMR imaging of multiphase flow in porous media, *AlChE J.*, *39*, 925–934.

Chen, Q., M. K. Gingras, and B. J. Balcom (2003), A magnetic resonance study of pore filling processes during spontaneous imbibition in Berea sandstone, *J. Chem. Phys.*, *119*, 9609–9616.

Chen W., J. Liu, F. Brue, F. Skoczylas, C. Davy, X. Bourbon, and J. Talandier (2012), Water retention and gas relative permeability of two industrial concretes, *Cem. Concr. Res.*, *42*(7), 1001–1013.

Christoffersen, K., and C. Whitson (1995), Gas/oil capillary pressure of chalk at elevated pressures, *SPE Form. Eval.*, *10*(3), 153–159.

Coates, G. R., L. Xiao, and M. G. Prammer (1999), *NMR Logging Principles and Applications*, Halliburton Energy Serv., Houston, Tex.

Colonna, J., F. Brissaud, and J. L. Millet (1972), Evolution of capillary and relative permeability hysteresis, *SPE J.*, *12*(1), 28–38.

Demond, A. H., and P. V. Roberts (1993), Estimation of two-phase relative permeability relationships for organic liquid contaminants, *Water Resour. Res.*, *29*(4), 1081–1090.

Dombrowski, H. S., and L. E. Brownell (1954), Residual equilibrium saturation of porous media, *Ind. Eng. Chem.*, *46*, 1207–1219.

Enwere, M. P., and J. S. Archer (1992), NMR imaging for water/oil displacement in cores under viscous-capillary force control, in *SPE/DOE Enhanced Oil Recovery Symposium*, Soc. of Petrol. Eng., SPE/DOE 24166, pp. 99–104. In: SPE/DOE 8th Symposium on EOR, Tulsa, Okla., 22–24April 1992.

Espinoza, D. N., and J. C. Santamarina (2010), Water-CO_2-mineral systems: Interfacial tension, contact angle, and diffusion: Implications to CO2 geological storage, *Water Resour. Res.*, *46*, W07537, doi:10.1029/2009WR008634.

Farokhpoor, R., E. G. B. Lindeberg, O. Torsæter, M. B. Mørk, and A. Mørk (2014), Permeability and relative permeability measurements for CO_2-brine system at reservoir conditions in low permeable sandstones in Svalbard, *Greenh. Gas. Sci. Technol.*, *4*, 36–52.

Fordham, E. J., L. D. Hall, T. S. Ramakrishnan, M. R. Sharpe, and C. Hall (1993), Saturation gradients in drainage of porous media: NMR imaging measurements, *AlChE J.*, *39*(9), 1431–1443.

Gallegos, D.P., K. Munn, D. M. Smith, and D. L. Stermer (1987), A NMR technique for the analysis of pore structure: Application to materials with well-defined pore structure, *J. Colloid Interface Sci.*, *119*(1987) 127–140.

Geffen, T. M., W. W. Owens, D. R. Parrish, and A. R. Morse (1951), Experimental investigation of factors affecting laboratory relative permeability measurements, *Pet. Trans. AIME*, *192*, 99–110.

Georgiadis, A., G. Maitland, J. P. M. Trusler, and A. Bismarck (2010), Interfacial tension measurements of the (H2O þ CO2) system at elevated pressures and temperatures, *J. Chem. Eng. Data*, *55*, 4168–4175.

Ghassemi, A., and A. Pak (2011), Numerical study of factors influencing relative permeabilites of two immiscible fluids through porous media using lattice Boltzann method, *J. Petrol. Sci. Eng.*, *77*(1), 135–145.

Gouze, P., and L. Luquot (2011), X-ray microtomography characterization of porosity, permeability and reactive surface changes during dissolution, *J. Contam. Hydrol.*, *120–121*, 45–55.

Huang, D. D., and M. M. Honarpour (1998), Capillary end effects in coreflood calculations, *J. Pet. Sci. Eng.*, *19*, 103−117.

Ishakoglu, A., and A. F. Baytas (2005), The influence of contact angle on capillary pressure–saturation relations in a porous medium including various liquids. *Int. J. Eng. Sci.*, *43*, 744–755.

Kleinberg, R. L., and J. A. Jackson (2001), An introduction to the history of NMR well logging, *Concepts Magn. Reson.*, *13*, 340–342.

Kleinberg, R. L., W. E. Kenyon, and P. P. Mitra (1994), Mechanism of NMR relaxation of fluids in rock, *J. Mag. Res. Ser. A*, *108*(2), 206–214.
Krevor, S., R. Pini, L. Zuo, and S. Benson (2012), Relative permeability and trapping of CO_2 and water in sandstone rocks at reservoir conditions, *Water Resour. Res.*, *48*, W02532, doi:10.1029/2011WR010859.
Lamy-Chappuis, B., D. Angus, Q. Fisher, C. Grattoni, and B. W. D. Yardley (2014), Rapid porosity and permeability changes of calcareous sandstone due to CO_2-enriched brine injection, *Geophys. Res. Lett.*, *41*, 399–406, doi:10.1002/2013GL058534.
Land, C. S. (1968), Calculation of imbibition relative permeability for two and three-phase flow from rock properties, *Soc. Pet. Eng. J.*, *8*(2), 149–156.
Lemmon, E. W., M. L. Huber, and M. O. McLinden (2013), *NIST Standard Reference Database 23: Reference Fluid Thermodynamic and Transport Properties-REFPROP*, Version 9.1, Natl. Inst. of Stand. and Technol., Stand. Ref. Data Program, Gaithersburg.
Lenhard, R. J., and J. C. Parker (1987), A model for hysteretic constitutive relations governing multiphase flow, 2. Permeability-saturation relations, *Water Resour. Res.*, *23*(12), 2197–2205.
Leverett, M. C. (1941), Capillary behavior in porous solids, *Trans. AIME*, *142*, 152–169.
Levine, J. S., D. S. Goldberg, K. S. Lackner, J. M. Matter, M. G. Supp, and T. S. Ramakrishnan (2014), Relative permeability experiments of carbon dioxide displacing brine and their implications for carbon sequestration, *Environ. Sci. Technol.*, *48*, 811−818.
McRobbie, D. W., E. A. Moore, M. J. Graves, and M. R. Prince (2006), *MRI from Picture to Proton*, Cambridge Univ. Press, Cambridge.
Meiboom, S., and D. Gill (1958), Modified spin-echo method for measuring nuclear relaxation times, *Rev. Sci. Instrum.*, *29*, 668–691.
Mitchell, J., T. C. Chandrasekera, D. J. Holland, L. F. Gladden, and E. J. Fordham (2013), Magnetic resonance imaging in laboratory petrophysical core analysis, *Phys. Rep.*, *526*(3), 165–225.
Mohr, P. J., B. N. Taylor, and D. B. Newell (2010), CODATA recommended values of the fundamental physical constants: 2010, *Rev. Mod. Phys.*, *84*, 1527–1605.
Morgan, J. T., and D. T. Gordon (1970), Influence of pore geometry on water-oil relative permeability, *J. Petrol. Technol.*, *22*, 1199–1208.
Morrow, N. R. (1976), Capillary pressure correlations for uniformly wetted porous media, *J. Can. Pet. Technol.*, *15*(4), 49–69.
Müller, N. (2011), Supercritical CO_2-brine relative permeability experiments in reservoir rocks: Literature review and recommendations, *Transp. Porous Media*, *87*(2), 367–383.
Olsen, D., S. Topp, A. Stensgaard, J. V. Nørgaard, and J. Reffstrup (1996), Quantitative 1D saturation profiles on chalk by NMR, *Magn. Reson. Imaging*, *14*(7), 847–851.
Parkhurst, D. L., and C. A. J. Appelo (2013), Description of input and examples for PHREEQC version 3: A computer program for speciation, batch-reaction, one-dimensional transport, and inverse geochemical calculations, *U.S. Geol. Surv. Tech. and Methods, Book 6*, Chap. A43, 497 pp.
Pentland, C. H., R. El-Maghraby, S. Iglauer, and M. J. Blunt (2011), Measurements of the capillary trapping of super-critical carbon dioxide in Berea sandstone, *Geophys. Res. Lett.*, *38*, L06401, doi:10.1029/2011GL046683.
Perrin, J.-C., and S. Benson (2010), An experimental study on the influence of sub-core scale heterogeneities on CO_2 distribution in reservoir rocks, *Transp. Porous Media*, *82*, 93–109.
Pini, R., and S. Benson (2013), Simultaneous determination of capillary pressure and relative permeability curves from core-flooding experiments with various fluid pairs, *Water Resour. Res.*, *49*, 3516–3530.
Pini, R., S. Krevor, and S. Benson (2012), Capillary pressure and heterogeneity for the CO_2/water system in sandstone rocks at reservoir conditions, *Adv. Water Resour.*, *38*, 48–59.
Pruess, K. (2005), ECO2N: A TOUGH2 fluid property module for mixtures of water, NaCl, and CO2, *Rep. 57952*, Lawrence Berkeley Natl. Lab., Washington, D. C.
Pruess, K., C. M. Oldenburg, and G. J. Moridis (1999), *TOUGH2 User's Guide*, Version 2.0. *LBNL Report LBNL-43134*, Lawrence Berkeley National Laboratory, Berkeley, Calif.
Ramakrishnan, T. S., and A. Cappiello (1991), A new technique to measure static and dynamic properties of a partially saturated porous medium, *Chem. Eng. Sci.*, *56*(4), 1157–1163.
Roberts, S. P., P. J. McDonald, and T. Pritchard (1995). A bulk and spatially resolved NMR relaxation study of sandstone rock plugs. *J. Magn. Reson. Ser. A*, *116*(2), 189–195.
Spiteri, E. J., R. Juanes, M. J. Blunt, and F. M. Orr (2008), A new model of trapping and relative permeability hysteresis for all wettability characteristics, *SPE J.*, *13*(3), 277–288.
Timur, A. (1969), Effective porosity and permeability of sandstones investigated through nuclear magnetic principles, *The Log Analyst 10(1)*, 3–11.
Vogt, S. J., C. A. Shaw, J. E. Maneval, T. I. Brox, M. L. Skidmore, S. L. Codd, and J. D. Seymour (2014), Magnetic resonance measurements of flow-path enhancement during supercritical CO2 injection in sandstone and carbonate rock cores, *J. Petrol. Sci. Eng.*, *122*, 507–514.
Wei, N., M. Gill, D. Crandall, D. McIntyre, Y. Wang, K. Bruner, X. Li, and G. Bromhal (2014), CO_2 flooding properties of Liujiagou sandstone: Influence of sub-core scale structure heterogeneity, *Greenh. Gas. Sci. Technol.*, *4*, 1–19.
Worden, R. H. (1998), Dolomite cement distribution in a sandstone from core and wireline data: The triassic fluvial Chaunoy formation, Paris Basin, in *Core-Log Integration*, edited by P. K. Harver and M. A. Lovell, *Geol. Soc. Spec. Publ., 136*, 197–211.
Zhao, Y., Y. Song, Y. Liu, H. Liang, and B. Dou (2011), Visualization and measurement of CO2 flooding in porous media using MRI, *Ind. Eng. Chem. Res.*, *50*(8), 4707–4715.
Zhu, Z., L. Mingyuan, L. Meiqin, S. Liang, and C. Long (2011), Investigation on variations in wettability of reservoir rock induced by CO_2-brine-rock interactions, paper SPE-142979-MS presented SPE EUROPEC/EAGE Annual Conference and Exhibition, Vienna, 23–26 May, doi:10.2118/142979-MS.
Zuo, L., S. Krevor, R. W. Falta, and S. M. Benson (2012), An experimental study of CO_2 exsolution and relative permeability measurements during CO_2 saturated water depressurization, *Transp. Porous Media*, *91*, 459−478.